JOURNAL OF AIRCRAFT
Vol. 45, No. 3, May–June 2008

Active Control of Three-Surface Aeroelastic Model

S. Ricci* and A. Scotti†
Politecnico di Milano, 20156 Milano, Italy
and
J. Cecrdle‡ and J. Malecek§
Aeronautical Research and Test Institute, 199 05 Praha 18-Letnany, Czech Republic

DOI: 10.2514/1.33303

The present paper describes research activities related to the Active Aeroelastic Aircraft Structures Project, fulfilled by Politecnico di Milano, dealing with the aeroelastic demonstrator named X-DIA. This aircraft is a one-tenth geometrically and dynamically scaled model of a regional transport airplane, and it has been built to become a wind-tunnel benchmark for experimenting with new aeroelastic concepts. All movable foreplane surfaces and wings with distributed multiple control surfaces are here installed to improve overall aeroelastic response and thus to improve airplane stability and even fuselage flight comfort. An identical location of accelerations and forces-based control system has been implemented: numerical and experimental results show a remarkable capability of this device in damping fuselage bending and torsion modes. The following pages will provide information about the research project, describing methodologies adopted and experiment results taken in wind-tunnel testing.

Nomenclature

C_s	=	generalized damping matrix
c	=	reference chord
$\mathbf{f}$	=	generic external aerodynamic force term
$\mathbf{f}_a$	=	generic unsteady aerodynamic force term
$H_{\text{ag}}(k, M_\infty)$	=	unsteady aerodynamic gust frequency response matrix
$H_{\text{am}}(k, M_\infty)$	=	unsteady aerodynamic frequency response matrix
K_s	=	generalized stiffness matrix
k	=	reduced frequency $= \frac{\omega \cdot c}{2V_\infty}$
M_s	=	generalized mass matrix
M_∞	=	Mach number
$\mathbf{q}$	=	generalized coordinate
$\boldsymbol{r}$	=	virtual states vector
V_∞	=	flight speed
x_a	=	aerodynamic states
ϑ_i	=	actuator axis rotation angle degree of freedom
ξ	=	modal damping added by active control

I. Introduction

DESIGN of efficient and safe new aircraft is one of today's goals for the aeronautic industry. The quest of realizing bigger, faster, and cheaper jetliners often shadows the importance of regional transport aircraft. These airplanes do suffer aeroelasticity as much as any other aircraft, and not often have active control been adopted on these machines to improve dynamic response, to reduce load effects on highly stressed parts, or just to improve flight cabin comfort. Structural modal control appears to be one of the possible solutions to significantly suppress negative aeroelastic effects, but aeronautic history is providing examples in which active control turned out to be very efficient in improving aircraft dynamic response, or when simple structural constraints (such as when highly flexible wings are used) can be a limit to aircraft performances. The XB-70 Valkyrie [1,2], B-52 [3], and B-1b [4] are clear examples of how the usage of modal control can exploit beneficial effects over structures, and the entire F-18 Active Adaptive Wing (AAW) project [5–7] shows how active control can be used to improve aeroelastic response and, at the same time, saving structural weight. Of course, these examples do refer to military aircraft, thus particularly enhanced dynamic behavior but similar problems are felt even when dealing with jetliners, as the quest for cheaper and more efficient flying machines often leads to unconventional and extreme shape and structural solutions. In 2003, a research and technological development (RTD) project started, partially funded by the European Union, under the key action aeronautics of the "Competitive and Sustainable Growth" RTD Program named "Active Aeroelastic Aircraft Structures" (3AS) [8]. The major objective was to improve aircraft efficiency by exploiting aeroelastic structural deformations in a beneficial way. The project consortium consists of 14 partners from the aeronautical industry, research establishments, and universities: Alenia (Italy), EADS-CASA (Spain), EADS-Deutschland, Aernnova (Spain) (Aeernnova was formerly known as: Gamesa Desarrollos Aeronuticos), Saab AB (Sweden), Centro Italiano Ricerche Aerospaziali S.C.p.A. (Italy), Deutsches Zentrum für Luft und Raumfahrt e.V. (Germany), Instituto Nacional de Tecnica Aerospacial (Spain), Vyzkumny a Zkusebni Letecky Ustav, a.s. (Czech Republic), Kungliga Tekniska Höskolan (Sweden), Instituto Superior Técnico (Portugal), Victoria University of Manchester (United Kingdom), Politecnico di Milano (Italy), Technion Research and Development Foundation, Ltd., (Israel), and, as a major subcontractor, the Central Aerohydrodynamic Institute (TsAGI) from Russia. The project aims to cover a wide range of potential aeroelastic concepts, tested for a number of preselected different demonstrator aircraft, for different classes of airplanes, ranging from a small remotely piloted vehicle (RPV) to a medium-range airliner and a wide-body transport aircraft. Among the others, a group of institutions represented by Politecnico di Milano, VZLU, DLR, and Alenia have been involved in investigating by means of both numerical and experimental activities, a "proof of concept": a three-surface medium-range airliner, referred to as target aircraft (TA) (see Fig. 1). A concept named active all-movable foreplane (later referred to only as AAMFP) has been installed on this aircraft: this concept relies on the usage of an additional lifting surface located on aircraft nose to control fuselage vibrations and to improve aerodynamic

Received 6 July 2007; accepted for publication 4 February 2008.

*Associate Professor, Dipartimento di Ingegneria Aerospaziale, Via La Masa 34; Sergio.Ricci@polimi.it. AIAA member.

†Ph.D. Fellow, Dipartimento di Ingegneria Aerospaziale, Via La Masa 34; scotti@aero.polimi.it. AIAA member.

‡Senior Scientist, Strength Research Department, Beranovych 130; cecrdle@vzlu.cz.

§Senior Scientist, Strength Research Department, Beranovych 130; malecek@vzlu.cz. AIAA member.

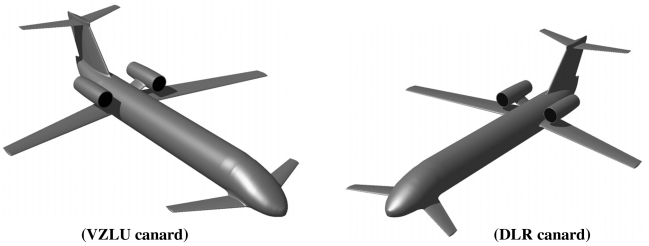

Fig. 1 CAD geometry of X-DIA aeroelastic demonstrator with forward-swept and backswept all-movable canard.

efficiency. To this end, a 1:10 aeroelastic scaled wind-tunnel model of the original airplane design, called X-DIA, and complete hardware–software foreplane control systems have been developed to perform all the experimental investigations and validations. In the following sections, all the analytical and experimental activities will be described, and the main investigation results, obtained during the 3AS project related to this unconventional configuration, will be summarized.

II. X-DIA Demonstrator

Some years ago, a scale model of a regional transport aircraft was designed, developed, and built at Dipartimento di Ingegneria Aerospaziale of Politecnico di Milano. This model was built with the purpose of evaluating on the field single- and multi-input parametric identification techniques, testing structural active control, and last but not least, testing stability augmentation systems [9]. One of the main problems faced during the design of aeroelastic models of an aircraft is matching all the relations implied by the quantity chosen to be held invariant between the model and the full-scale aircraft. The realization of an exact similitude demands reliable design and fabrication techniques to retain the experimental results as representative of the behavior of the full-scale aircraft: this statement affects the costs required to develop a wind-tunnel aeroelastic model or a dynamic flying model separately. It can be easily understood how complexity is destined to grow in the case of a flying aeroelastic model. Here, just the inspiring design philosophy of the X-DIA project is briefly recalled. The maximum takeoff weight was sized to fit the required payload (mainly sensors, acquisition, and control systems), whereas technological considerations led to the scaling factor, the Froude number being held invariant between the model and the full-scale aircraft because of the importance of the ratio between inertial and gravitational forces when flying at such a low speed. The model was designed as representative of a one-tenth-scale model of a short range liner in terms of dimensions, weights, and moments of inertia. On this model, an aeroelastic wing has been designed to have its natural scaled frequencies close to the typical wing frequencies of an aircraft of this class. Into the framework of the 3AS project, the original X-DIA RPV has been modified to be used as a wind-tunnel aeroelastic model to investigate mainly the AAMFP concept [10] used to improve the benefits of the three-surface configuration [11–14] and described in the following section. Even if studying and optimizing aircraft configurations was not among the main goals of the research, an unconventional three-surface configuration has been adopted. The scientific debate on the superiority of unconventional, canard, and three surface with respect to conventional design has received great attention in past years: the enthusiasm of some researchers, who claimed a three-surface configuration using both fore and aft as trimming surfaces can improve cruise efficiency in a stable trimmed condition over a practical range of gravity center positions, followed by the conventional and lastly by the canard configuration, has been impaired by theoretical and experimental works, which confirm the superiority of conventional design with respect to three-surface and canard configuration in the order. The aeroelastic demonstrator X-DIA is a Froude scaled model [15] (with a geometric scale factor of 1:10) designed and built at Politecnico di Milano using a constructive typology based on beams to reproduce fuselage and wing stiffness distribution, whereas various aerodynamic sectors are reproducing

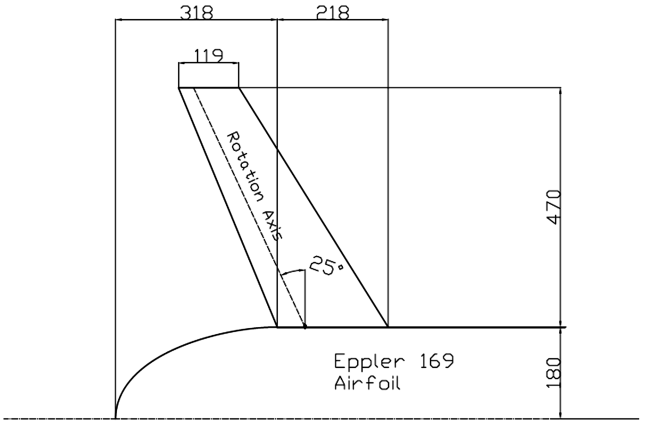

Fig. 2 Canard all-movable surfaces configurations: DLR type plant.

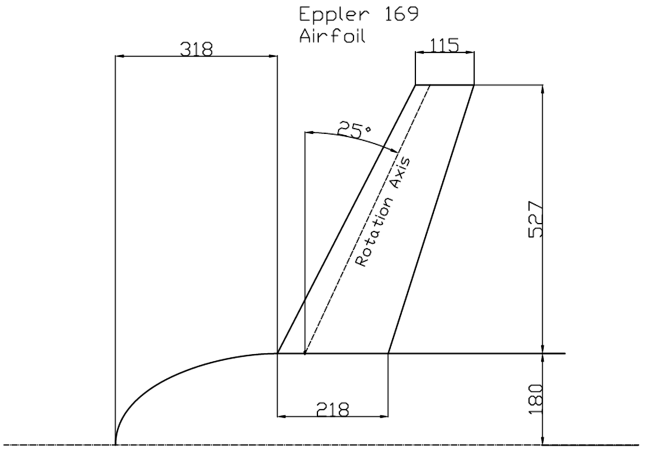

Fig. 3 Canard all-movable surfaces configurations: VZLU type plant.

external airplane shape. The demonstrator is composed of different modules that can be assembled together to investigate different aeroelastic concepts, as follows:

1) Front fuselage: Froude scaled with respect to the reference aircraft, based on an aluminum square tube connecting eight aerodynamic sectors made by carbon fabric and nomex.

2) Rear fuselage: rigid, equipped with vertical and T-Tail planes.

3) *Gray wing*: Froude scaled with respect to reference aircraft, based on an omega shape aluminum beam and 20 aerodynamic sectors made by styrofoam and Kevlar. This wing is equipped with one aileron.

4) *Black wing*: Froude scaled with respect to reference aircraft, it features a single spar, carbon fabric made, with a hollow cross-section shape and 20 aerodynamic sectors made by styrofoam covered by carbon fabric. The wing is equipped with eight control surfaces (four leading edge and four trailing edge) thus permitting a sort of discrete "variable wing camber." This solution permits, by using common control surfaces, modal control over the wing, improved maneuverability, and, of course, an improved aircraft flutter envelope.

5) Foreplanes: two kinds of foreplanes, similar in terms of wetted surface, but different in terms of sweep angle. The first one is forward swept whereas the second is backward swept, and they are designed and manufactured by VZLU and DLR, respectively (see Figs. 2 and 3). Both wings of each foreplane are moved by the same control system based on two independent electric brushless motors connected to the wings through a belt-driven transmission (see Fig. 4).

III. Aeroelastic Concepts

On such an innovative configuration, different aeroelastic concepts can be tested, but one among the variety studied during 3AS

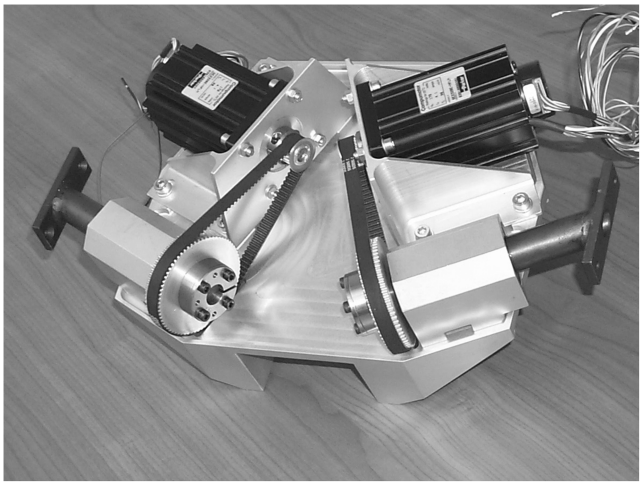

Fig. 4 All-movable foreplane actuator system.

project, the AAMFP [10], is deeply investigated by means of either numerical models or wind-tunnel testing. The addition of all-movable control surfaces right on the nose cone of an aircraft, can lead to some benefits such as providing significant improvements in terms of gust alleviation, reduction of fuselage vibrations by active control, and minimization of overall trim drag taking aeroelastic deformations into account. Of course, due to high cruise speed, this aerodynamic additional surface must either be back swept or must use the benefits provided by aeroelastic tailoring and thus show a forward-swept planform [16]. To understand which of these solutions can provide better aeroelastic response, two different foreplanes have been studied and installed on the aeroelastic demonstrator X-DIA (see Figs. 2 and 3). These two foreplanes have been used to replace the original fixed foreplane already present on the aircraft, and the same active control system will be adopted when testing the model inside the wind tunnel. The benefits of the AAMFP concept were investigated both numerically and experimentally using an X-DIA component model only, that is, front fuselage equipped with both foreplanes and the complete X-DIA model, respectively.

IV. Methodology Adopted and Numerical Setup

The scheduled programs of 3AS were organized to test, at first, the benefits of the AAMFP concept on an aircraft component (thus by evaluating only the effects of forewing over fuselage only) and later to test the concept on the whole aircraft (this setup involved the complete aircraft in free-flight cruise condition). Numerically speaking, this compelled the realization of different models that had to reproduce correctly the dynamics of the model under evaluation, together with the (hardware) testing apparatus involved. Finite element method (FEM) models realized with MSC-NASTRAN software were used to model structures and aerodynamics, and reduced-order models were thus built by means of an "in-house" code developed to design and develop control systems. These reduced-order models are strictly based on mass, stiffness, damping, and aerodynamic matrices obtained by NASTRAN. These matrices are easily obtained with a methodology already presented by the same authors in [17]. The result of this procedure is a state-space system of dynamic equations, which generates, when given modal degrees of freedom of the structure as input, the generalized aerodynamic forces as output. This system can be connected in feedback with the structural model to obtain a complete time domain aeroelastic model. This model has been used to design a controller using a Matlab Simulink environment.

A. Reduced-Order State-Space Models

The unsteady aerodynamic loads due to small structural motions and gusts are usually obtained as solutions of integro-differential equations related to harmonic boundary domain oscillation, which leads to the generalized aerodynamic forces frequency response. The current practice is still based on the numerical evaluation of the transfer matrix on the imaginary axis, because the analytic continuation may be called into play to justify the extension of the data known on the imaginary axis. Various formulations for the rational approximation of aerodynamic transfer function have been developed (see [18–23]). In any case, the starting point is the knowledge of the generalized aerodynamic forces:

$$\mathbf{f} = \mathbf{H}_{\text{am}}(k, M_\infty) \cdot q + \mathbf{H}_{\text{ag}}(k, M_\infty) \cdot \frac{V_g}{V_\infty} \tag{1}$$

Roger [19] proposed to approximate those matrices as

$$\mathbf{H}(p) \simeq \mathbf{D}_0 + \mathbf{D}_1 p + \mathbf{D}_2 p^2 + \sum_{i=1}^{m} \frac{p}{p + \beta_i} \mathbf{E}_i \tag{2}$$

where the poles $-\beta_i$ are prescribed by the user in the range of interest of p and are real and negative to ensure the stability of the dynamic system. All the coefficients are evaluated using a least-squares technique on each individual term. The resulting model for the aerodynamic generalized forces has an $m \times n$ dimension, where n is the number of structural generalized degrees of freedom. Roger's technique is straightforward, robust, easy to implement, and inexpensive in terms of computational burden. However, it requires a significant increase in the states number to improve the accuracy: the addition of a new pole requires one to increment the state number by n. Roger's technique is not the only possibility to obtain reduced-order models: literature offers many examples of techniques (see, for instance, Karpel [20] and also Morino et al. [23], who propose a sort of multipoint Padé approximation) that can permit achieving good results with quite a reasonable computational effort, especially with today's computers.

During this work, the procedure adopted joins the simplicity and robustness of Roger's method with the balanced truncation reduction methods [24] to recover small compact models for the aerodynamic generalized forces. The first step is characterized by the creation of an accurate but large state-space (StSp) model using a high-order Roger's approximation, Eq. (2), which must be capable of reproducing all the details of the given transfer matrices. System poles $-\beta_i$ are usually assigned as evenly distributed points within the given range of reduced frequencies. However, when this range happens to be large, a great improvement in fitting quality may be obtained by running a simple optimization on pole positioning to minimize the local relative error. The optimization process is usually very fast because a very small set of parameters is involved.

Once an high-order StSp model, which accurately represents the dynamics of the generalized aerodynamic forces, is obtained, a classical model reduction technique is used, as already suggested in [23]. The main elements, which must be satisfied by the reduction technique, are to 1) obtain a measurable and *small* global error, 2) preserve stability, and 3) require a reasonable computational effort.

Being the state matrix diagonal and full rank, it is likely that any order reduction will be related to a lack of controllability/observability. Here the classical balanced truncation model reduction algorithm has been used. The method tries to reduce the $\mathcal{H}_\infty$ norm of the system, which is a measure of the largest possible energy increase between inputs and outputs (see [25]). First of all, it is necessary to build the *controllability gramian*

$$\mathbf{G}_c = \int_0^{+\infty} e^{\mathbf{A}t} \mathbf{B}\mathbf{B}^* e^{\mathbf{A}^* t}\, \mathrm{d}t \tag{3}$$

which contains all the dynamics that are reachable by the system inputs, and the *observability gramian*

$$\mathbf{G}_o = \int_0^{+\infty} e^{\mathbf{A}^* t} \mathbf{C}^* \mathbf{C} e^{\mathbf{A}t}\, \mathrm{d}t \tag{4}$$

which instead contains all the observable dynamics of the system. These gramians are the solutions of the two following Lyapunov equations:

$$\mathbf{A}\mathbf{G}_c + \mathbf{G}_c\mathbf{A}^* + \mathbf{B}\mathbf{B}^* = 0 \tag{5}$$

and

$$\mathbf{A}^*\mathbf{G}_o + \mathbf{G}_o\mathbf{A} + \mathbf{C}^*\mathbf{C} = 0 \tag{6}$$

If these two gramians are two positive definite matrices, then there always exists a linear transformation T (see Moore [25]) such that the two transformed gramians are both diagonal and equal to

$$\hat{\mathbf{G}}_c = \hat{\mathbf{G}}_o = \mathrm{diag}\{\sigma_1, \sigma_2, \ldots, \sigma_{n\text{-}m}\} \tag{7}$$

In this case, σ_i are the square roots of the eigenvalues of the product of the two gramians and are called *Hankel singular values* (HSV). Usually, the HSVs decay extremely rapidly, meaning that low-order accurate model are possible. The reduced model is obtained by simply truncating the system to the first k modes of the transformation matrix T. The $\mathcal{H}_\infty$ norm of the system is bounded by the value

$$2\sum_{i=k+1}^{m\cdot n}\sigma_i$$

In this way, it is possible to obtain a reduced-order model of the original large system, which represents the aerodynamic forces at a very low cost. The technique has the additional advantage to yield simultaneously all reduced model of degree 1 up to $m \cdot n$. To improve the quality of the reduced-order model in the low-frequency range, we enforce an exact fit of the real part and of the slope of the aerodynamic forces transfer function at zero reduced frequency. This can be done by applying a dynamic residualization of fast-system dynamics [26]. More details on the procedure sketched here may be found in [27].

The technique described in the previous lines is here applied to the DLR and VZLU canard equipped X-DIA front fuselage model. The starting frequency domain data are based on a 15 flexible modes model analyzed in a large range, from 0.001 to 5.0, of reduced frequencies. Results are shown for two characteristic coefficients of the H_{am} matrix. The first case presented is dealing with the coefficient (2, 2) related to the first antisymmetric fuselage torsional mode, as reported in Fig. 5; the second example presented is dealing with the coefficient (2, 7), which relates the inputs on mode 7 to the generalized force on mode 2, Fig. 6. A Padé first-order approximation is compared with different models obtained by the sketched procedure. Figures 5 and 6 are showing, respectively, a complete fifth-order Roger's model; the model obtained by running the pole positioning optimization; a reduced model made by 17 states, which appears to be the minimal dimension for the system looking at the HSV behavior; and a 22 states reduced model. For the coefficient (2, 2), which is a leading coefficient in terms of magnitude, all the models give comparable results; small differences can be highlighted in the behavior of the real part at high reduced frequencies, in which all Roger's models appear to match better the original data. The case of the coefficient (2, 7) gives more information on the differences among the different models. The Padé fitting completely misses the coefficient behavior, generating large spurious oscillations; rising approximation order leads to unstable models. The fifth-order Rogers approximation gives better results, even though an incorrect oscillation may be seen in the coefficient real part. This is completely wiped out by running the optimization process, which recovers a very good fitting. Reducing the model by balanced truncation to 17 states, the optimal indication given by the HSV allows the correct reconstruction of the leading coefficient (2, 2) but leaves a spurious oscillation on coefficient (2,7). Rising system dimensions to 22 gives the optimal reduced-order model, which has been here used for the control system synthesis and analysis.

After determining the state-space aerodynamic system [Eq. (2)], a set of state-space equations describing the aeroelastic system model were drawn and have the form [Eq. (8)]

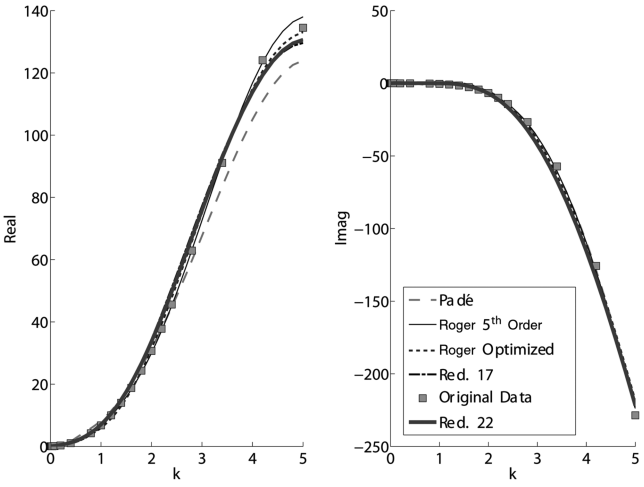

Fig. 5 Frequency domain aerodynamic transfer matrix, coefficient (2,2).

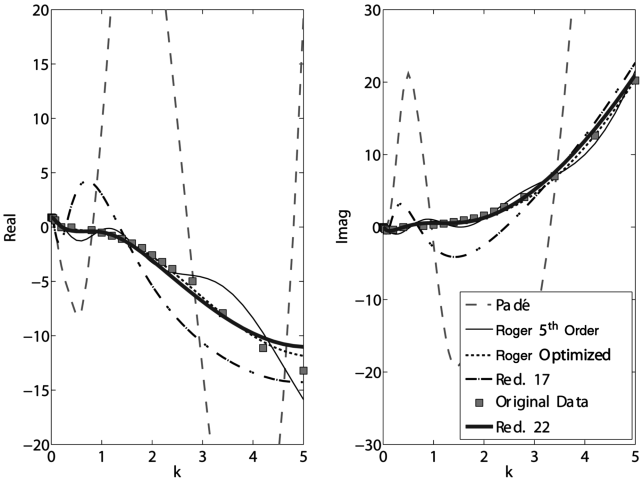

Fig. 6 Frequency domain aerodynamic transfer matrix, coefficient (2,7).

$$\begin{cases} \dot{\mathrm{x}} = A\mathrm{x} + B\mathbf{u} \\ \mathrm{y} = C\mathrm{x} + D\mathbf{u} \end{cases} \tag{8}$$

Each generalized structural degree of freedom was necessarily represented by two states $\mathbf{q}$ and $\boldsymbol{r}$ so as the aeroelastic system model could be described as follows [Eq. (9)]:

$$E_{\mathrm{ae}}\dot{\mathrm{x}}_{\mathrm{ae}} = A_{\mathrm{ae}}\mathrm{x}_{\mathrm{ae}} + B_{\mathrm{ae}}\mathbf{f} \tag{9}$$

The described terms E_{ae}, A_{ae}, and B_{ae} are defined as follows:

$$E_{\mathrm{ae}} = \begin{bmatrix} M_{\mathrm{ae}} & 0 & 0 \\ 0 & I & 0 \\ 0 & 0 & I \end{bmatrix}, \quad A_{\mathrm{ae}} = \begin{bmatrix} -C_{\mathrm{ae}} & I & 0 \\ -K_{\mathrm{ae}} & 0 & qC_a \\ (V_\infty/c)B_{\mathrm{am}} & 0 & (V_\infty/c)A_{\mathrm{am}} \end{bmatrix}$$

$$B_{\mathrm{ae}} = \begin{bmatrix} 0 \\ I \\ 0 \end{bmatrix}$$

To build these matrices, it is also required to define M_{ae}, C_{ae}, and K_{ae} in the following way:

$$M_{\mathrm{ae}} = M_s - q(c/V_\infty)^2 D_{2\mathrm{am}}$$
$$C_{\mathrm{ae}} = C_s - q(c/V_\infty)^2 D_{1\mathrm{am}}$$
$$K_{\mathrm{ae}} = K_s - qD_{0\mathrm{am}}$$

and

$$\mathrm{x}_{\mathrm{ae}} = \begin{Bmatrix} \vartheta_0 \\ \vartheta_1 \\ \mathbf{q} \\ \vartheta_{0r} \\ \vartheta_{1r} \\ \boldsymbol{r} \\ \mathrm{x}_a \end{Bmatrix}$$

where θ_0 and θ_1 are actuator axis rotation angles (left and right), and the virtual state vector $\boldsymbol{r}$ is defined by

$$\boldsymbol{r} = M_s\dot{\mathbf{q}} + C_s\mathbf{q} - q(c/V_\infty)^2 D_{2\mathrm{am}}\mathbf{q} - q(c/V_\infty)D_{1\mathrm{am}}\mathbf{q} \qquad (10)$$

It is still possible to compute, by the state system, the accelerometer measurement outputs that will be used as direct feedback of the active control system. Those are computed by modal participation of nodes placed corresponding to accelerometers along the desired direction.

B. Identical Location of Accelerations and Forces (ILAF) Control Scheme

A brief description of the logic chosen for active control on foreplanes is now requested: no new specialized high-performance systems were adopted, but, simply, the well-known ILAF principle, which is easy to implement. This system was first designed and installed by NASA on the XB-70 airplane in the 1970s. This concept requires the application of a force proportional to the local structural velocity (this explains the acronym) just in the same location and in the direction in which structural velocity is measured [1,2]. In this way, the active control system simply operates as a passive damper. The configuration adopted for the model and the long fuselage offered a perfect platform for the application of this kind of stability control system. NASA planned this particular system to provide stability augmentation during climb out at a high subsonic speed and in a heavyweight condition on an airplane with high fuselage flexibility. The selection of this system compared with others was mainly due to the fact that its implementation is very simple: few accelerometers and a straight control architecture are very important. Moreover, accelerometers are quite useful and common sensors, and so it was expected that their usage could be extended and good results could be achieved both in case of continuous turbulence and of discrete gusts.

V. Experimental Setup and Model Description

The experimental activities related with 3AS took place in two different locations, Prague and Milano, where two wind tunnels were prepared to test the aeroelastic demonstrator X-DIA in two different configurations. The following paragraphs will provide a brief description of the wind tunnel used and about the model and its installation.

A. Wind-Tunnel Facilities

The demonstrator has been tested at first at VZLU in Prague (Czech Republic). The wind tunnel is a low-speed, closed-circuit type with an open circular test section of 3-m diameter and 3-m length. The maximum air speed is 70 m/s. During this first wind-tunnel test session, only aircraft fuselage equipped with foreplanes has been installed on a very stiff boom: this installation was realized to line out basic characteristics of the control system and to check out the effectiveness of the canard wing on the fuselage itself. The second facility where wind-tunnel testing took place is located at Politecnico di Milano. This installation presents a closed circuit wind tunnel and offers both capability of closed and open test sections. The closed test chamber that was used during the test campaign has the following dimensions: 4×4-m cross section and 5-m length. Air speed can reach up to 60 m/s. Here the model has been installed in "complete" configuration, using a free–free suspension system.

B. Control Surfaces: Foreplanes

As already mentioned, the model has been equipped with two different all-movable foreplanes. Figures hereafter mentioned present the two final configurations adopted during test (DLR Fig. 2 and VZLU Fig. 3, respectively). These two solutions are very different in sweep angle (± 25 deg) and slightly different in overall span and mass distribution. Structural design was based on the requirements of the wind-tunnel test conditions. The forward-swept foreplane was designed in such a way that the wash-in effect due to sweep was compensated by a suitable orientation of the fiber material. Anyway, both surfaces can provide the same pitching moment about the aircraft c.g. and are thus fully comparable. Both foreplanes are attached to a torsion tube centered at quarter chord line. This device has a double function: it connects the foreplanes to the fuselage and transmits the actuator motion to the all-movable surfaces. A specially designed drive system has been realized for this purpose. Electric brushless motors and encoders were used together with corresponding decoders.

C. Control System and Instrumentation

A special control system for the X-DIA model has been designed and built at Politecnico di Milano. An off-the-shelf PC running an RTAI-Linux OS has been used to perform both model control and data acquisition. The specific control system has been implemented under Matlab Simulink. Specific details can be found in [10]. This system has the capability to actuate independently both canard surfaces, allowing both a common static trim of the model and also active control of fuselage symmetric bending modes (a symmetric rotation of the foreplane produces a lift sufficient to damp fuselage bending) as well as antisymmetric modes (in this case, antisymmetric rotation produces a torque to damp fuselage torsion). The same control system is also capable of excitation: a special sweep run in a specified relevant frequency range has been implemented to actuate the foreplane (both in symmetric and antisymmetric ways).

Model instrumentation is realized as follows: two 1000-line encoders are attached to the foreplane torsion tubes and allow measurement of the control surface rotations, two integrated-circuit piezoelectric (ICP) accelerometers placed on the tips at quarter chord provide vertical acceleration measurements and detection of symmetric and antisymmetric fuselage modes. Additional accelerometers are placed all over the model: two of them are installed on the fuselage nose sensing in vertical and lateral direction. These sensors are not used by the control system but are simply used as most representative indicators of fuselage motion. When testing the complete model, one accelerometer is located at the aircraft center of gravity together with a capacitive triaxial accelerometer. The former is directly used by the active control system (because measurement of model c.g. acceleration is needed). The latter is used to evaluate aircraft angle of attack while using the soft suspension system. Instrumentation is completed by strain gauges placed on the fuselage main beam to measure shear strains and by three rate gyros to constantly measure airplane angular rates during the wind-tunnel test.

VI. Preliminary Simulations and Results

The previously described aeroelastic model in Sec. IV.A is a continuous state-space model. Some initial analysis were run with this model to investigate just the basic structural behavior. Later, the reduced order model (ROM) (and thus the StSp model) was updated by means of ground vibration testing and using LMS CADA-X software. The entire model has been tuned taking into account actuator bandwidth limits (measured experimentally), acquisition board limits, possible noise on signal lines, and possible nonlinearities (such as dead band and saturations present in the control system plant). This allowed the creation of a complete simulator, which is presented in Fig. 7. The state-space ROM block contains the state-space model and is connected to the rest of the simulator through some zero-order hold, replicating the sampling time as present on the physical model. The StSp model features three inputs (see Fig. 7): torque sent to both motors and excitation (here

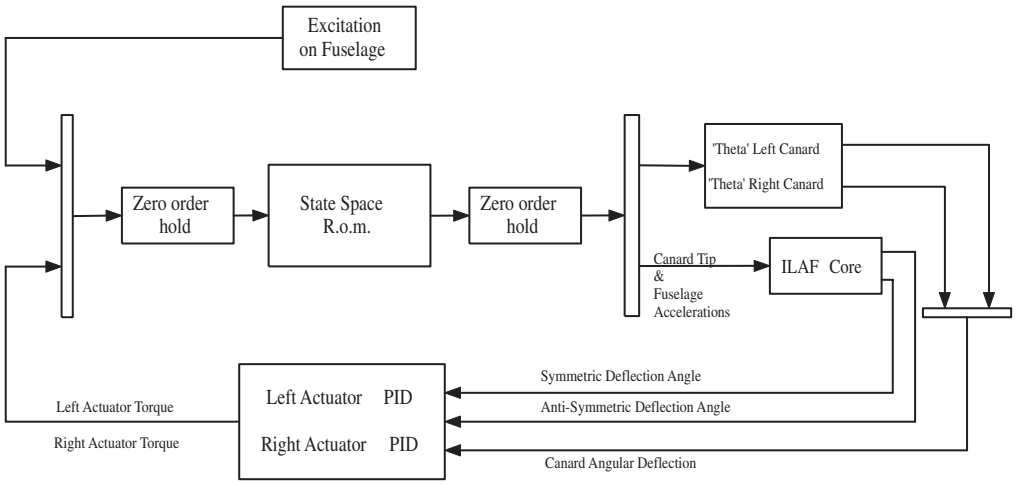

Fig. 7 Numerical model block diagrams: Simulink simulator.

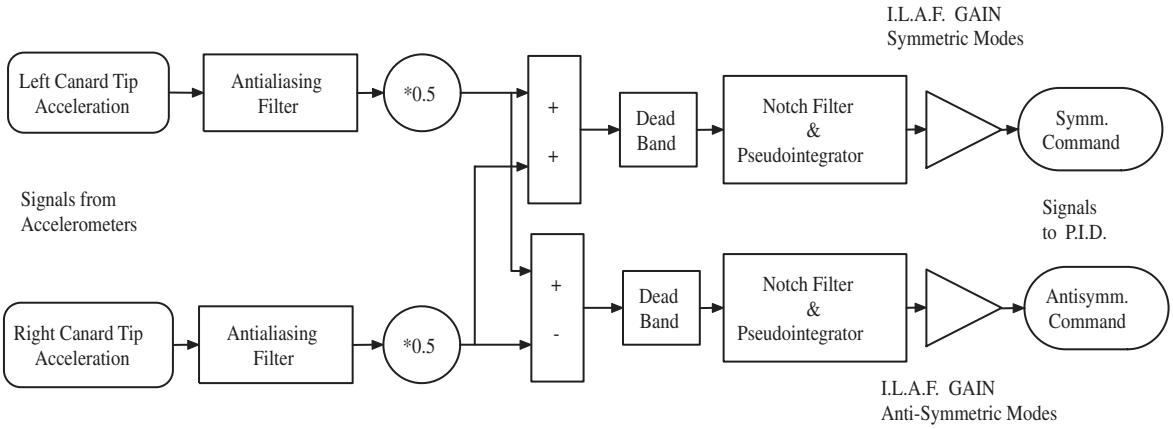

Fig. 8 Numerical model block diagrams: ILAF Simulink core scheme.

reproducing a special sweeplike frequency sampled force introduced on one side of fuselage). The outputs of this model are, respectively, the accelerations measured on some important points (such as foreplane tip and fuselage nose) and angular deflection of each all-movable foreplane. Former signals are processed by the ILAF block: a simple pseudointegration allows evaluating structural velocity (see Fig. 8) and generation of the subsequent command signal (thus, foreplane deflection angle is directly proportional to structural velocity). The latter are introduced into a proportional, integral, derivative (PID) block as encoder reading of the foreplane deflection.

VII. Wind-Tunnel Testing Results

The following lines provide only some significant results obtained during the wind-tunnel test sessions. The first part of wind-tunnel testing took place at VZLU in Prague with a component model consisting of the front fuselage and two different foreplanes. The first wind-tunnel entry was in March 2004. At first, static characteristics of the component model have been determined, both with wind-off static load tests and later with aerodynamic loads. Stability derivatives and lift/drag polars were evaluated involving both foreplane configurations and fuselage itself only. These data were useful in later updating of the reduced state-space aeroelastic models and for tuning the active control system. A second wind-tunnel entry took place again at VZLU, this time aiming at active control experiments: both foreplane configurations were tested on the front fuselage.

A. Component Model

In the following lines, results of tests performed at VZLU in Prague are presented [28–30]. At first, the model was attached to a 6 degrees of freedom balance, and static tests have been performed aimed at measuring control effectiveness of two different type of foreplanes, fuselage deflection underloading using a laser-based system together with photogrammetry, and maximum static torque allowable by the foreplane's control system. Then the model was detached from the balance and connected by means of a stiff sting support. In this particular configuration (Fig. 9), modal analysis showed a clear separation between fuselage modes. In Table 1, the measured eigenfrequencies related to fuselage bending and torsion modes are listed. This is the particular frequency range in which the

Table 1 X-DIA component model: modal parameters

DLR foreplane		VZLU foreplane	
Mode no.	Frequency, Hz	Frequency, Hz	Mode shape
1	3.689	3.841	First vertical fuselage bending
2	4.697	5.158	First horizontal fuselage bending
3	19.100	21.650	First fuselage torsion
4	31.490	31.650	Second vertical fuselage bending

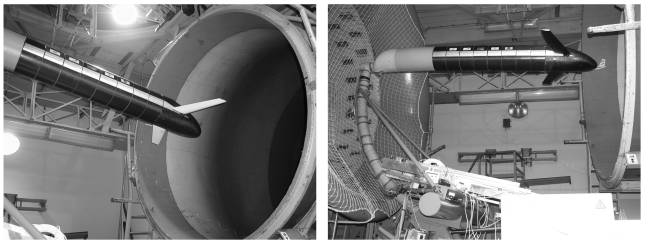

a) Fuselage with DLR Canard b) Fuselage with VZLU Canard

Fig. 9 Fuselage sting support at VZLU wind-tunnel facility.

active control is operative. Finally, after completing this first testing session, a second session was started, mainly focused on active control efficiency evaluation. To excite the component model, a hydraulic excitation device was installed and connected to the left side of the fuselage so as to be able to excite both bending and torsion modes. In particular, two frequency sweeps, from 3.5 to 4.5 Hz and from 14 to 22 Hz, have been used to excite fuselage bending and torsion, respectively. The main object of dynamic testing is the evaluation on AAMFP performances, and this could be obtained comparing the measured transfer functions between the fuselage response (obtained measuring the acceleration of nose cone and foreplane tip) and the input force for different speeds ranging from 10 to 35 m/s and ILAF control gains. At first, an excitation was used to activate bending and torsion modes separately. Later, both types of modes were excited, and the control system tuned to operate in a mixed symmetric and antisymmetric way. Figures 10–13 report, for example, the measured accelerations on the nose cone and foreplane tips for two types of foreplanes at a speed of 25 m/s and for different gain values compared with ones obtained using the aeroelastic simulator described in the previous section. Looking at these results, it is possible to see the effectiveness of the control system in damping fuselage-bending vibrations. A clearer view of canard efficiency in damping fuselage modes of the clamped fuselage is proposed in Figs. 14–17, in which gain effectiveness, computed as extra modal damping on measured transfer functions (i.e., nose cone and foreplane tip vertical accelerations over input force, expressed as H1 estimators), is reported at different speeds: even in this case, the experimental results are compared with the numerical ones. These figures report allowable values by test and numerical simulation and interpolation lines as cubic polynomials in a least-squares sense. When active control deflects symmetrically canard foreplanes, control is related to fuselage-bending mode, and the ILAF control system appears very efficient for both DLR and VZLU foreplanes. The maximum damping, equal to 2.2%, is obtained for VZLU foreplane, at a speed equal to 35 m/s and for a gain equal to 10. It clearly appears that the only difference between the two canard configurations is the maximum value that allows obtaining the same amount of acceleration reduction, as both solutions almost come to the same achievement. Looking at the damping values predicted by the numerical model, it appears that the overall trend is well captured even if a small difference still remains: in general, damping factors predicted by the numerical model are lower than ones measured during the wind-tunnel test on the component model. When dealing with asymmetric control related to fuselage torsion, some attenuation can be obtained only when operating with DLR foreplane. Looking at Fig. 16, it appears that with the DLR foreplane, it is still possible to achieve a certain value of damping (at maximum value equal to 1%) but damping value decreases when increasing flying speed, and this appears as a symptom that operating condition is close to control system instability, which rises immediately for gain = 1 at a flying

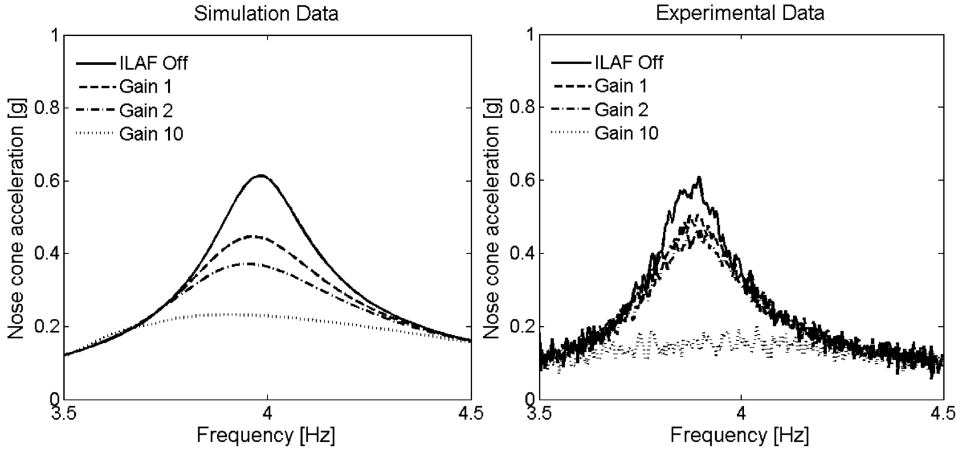

Fig. 10 Symmetric control. VZLU foreplane simulation results (left) vs experimental results (right).

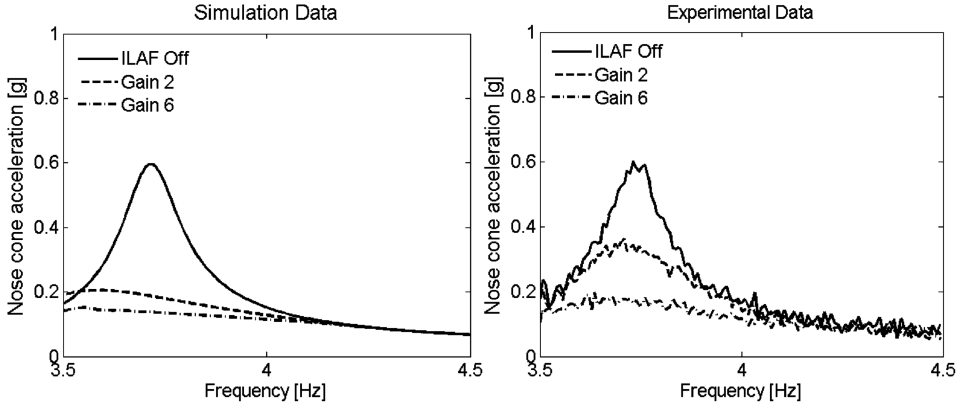

Fig. 11 Symmetric control. DLR foreplane simulation results (left) vs experimental results (right).

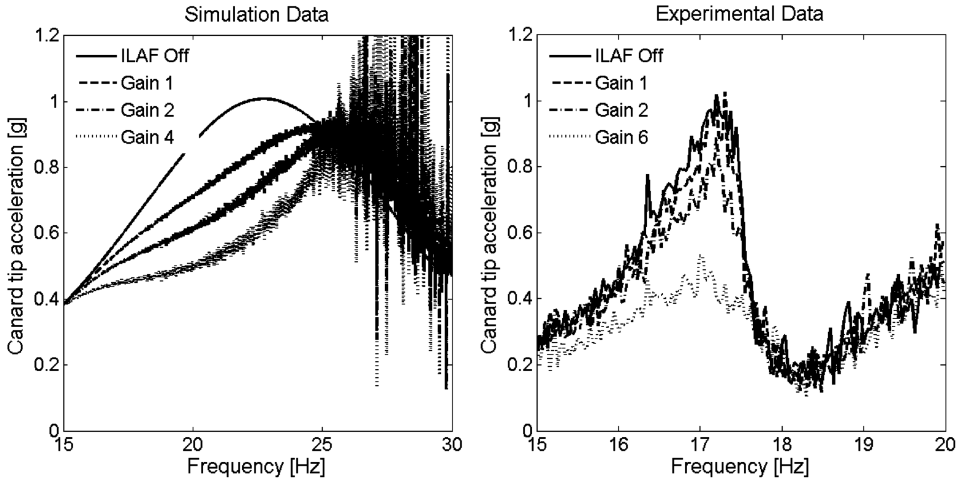

Fig. 12 Antisymmetric control. DLR foreplane simulation results (left) vs experimental results (right).

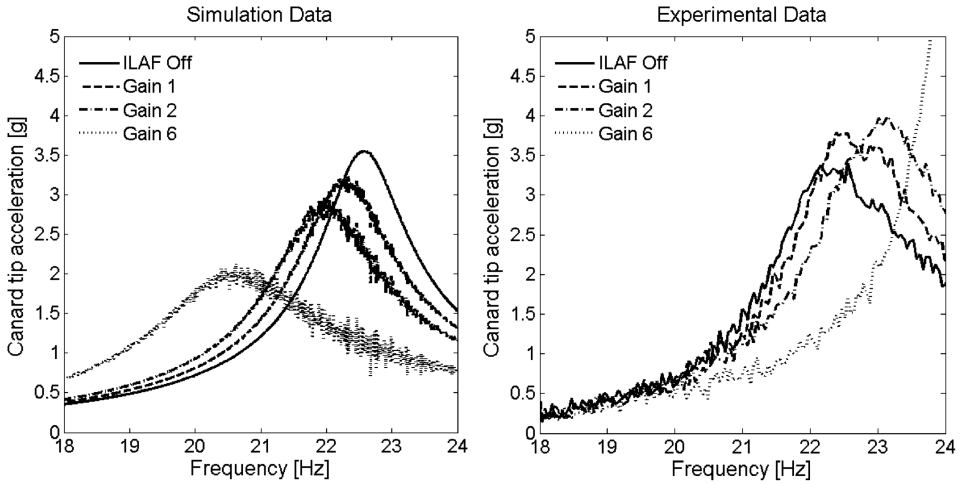

Fig. 13 Antisymmetric control. VZLU foreplane simulation results (left) vs experimental results (right).

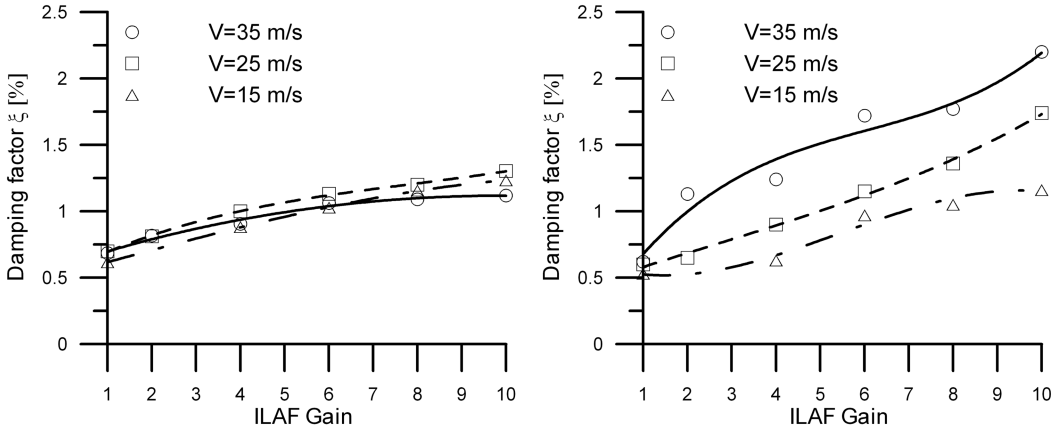

a) Numerical **b) Experimental**

Fig. 14 Numerical vs experimental gain effectiveness for symmetric control on X-DIA front fuselage: VZLU foreplane.

speed of 40 m/s. The numerical models, like in the case of symmetric control, slightly underestimate the damping values. When operating with VZLU foreplane, as appears looking at Fig. 13 and 17, a very small attenuation is possible, and control instabilities for increasing speed and gain are reached very soon, for gain = 2 at 20 m/s or for gain = 1 at 25 m/s. A reason for this inefficiency is surely related to the frequency of fuselage torsion mode when connected to different type of foreplanes. In fact, when DLR foreplanes are installed, the weight effect of these canard wings leads fuselage torsion frequency drop to 19.10 Hz, well beyond the maximum bandwidth of control system. Otherwise, in the case of VZLU canard wings, fuselage torsion mode shows a frequency of 21.65 Hz, and this value is very close to the maximum allowable bandwidth of the control system.

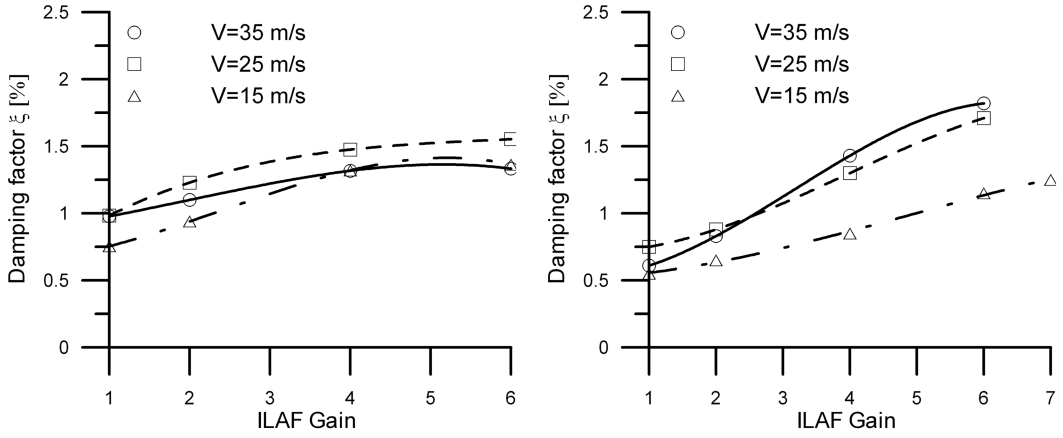

a) Numerical b) Experimental

Fig. 15 Numerical vs experimental gain effectiveness for symmetric control on X-DIA front fuselage: DLR foreplane.

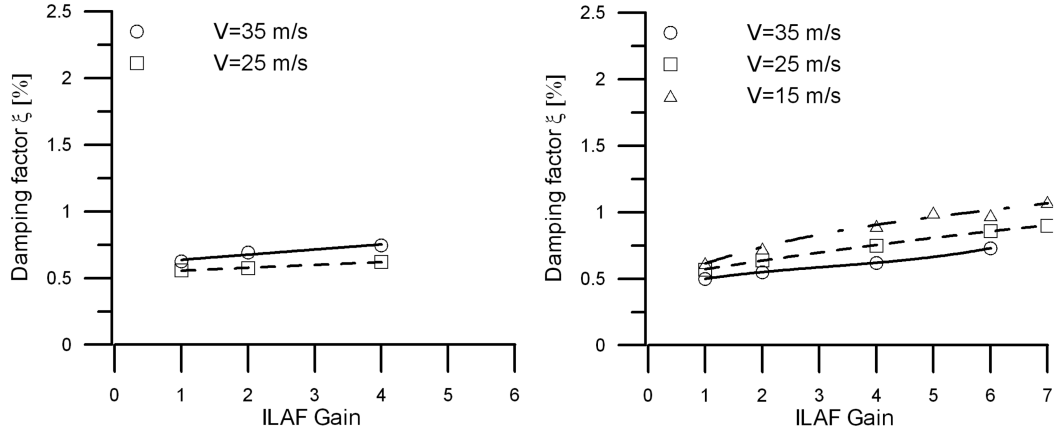

a) Numerical b) Experimental

Fig. 16 Numerical vs experimental gain effectiveness for asymmetric control on X-DIA front fuselage: DLR foreplane.

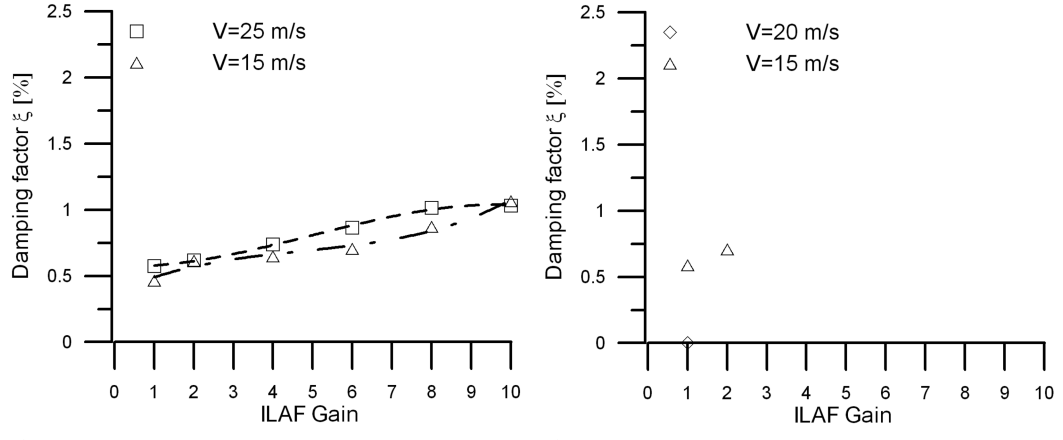

a) Numerical b) Experimental

Fig. 17 Numerical vs experimental gain effectiveness for asymmetric control on X-DIA front fuselage: VZLU foreplane.

Additional results related to the experimental activity here presented, dealing with some intermediate velocities can also be found in [31], where a more detailed description of the testing activity has been presented.

B. Complete Model

The wind-tunnel testing on the complete model, that is, on front and rear fuselage equipped with vertical and T-Tail planes, gray wing, and foreplanes, was performed at Politecnico di Milano. The model has been supported by a soft suspension system similar to the one used at TsAGI, but with some modifications [32]. The main differences with respect to the original system are the following: in this case, only one cable is connected to the front fuselage, and two cables with springs are attached to the fuselage close to the nodes of its first bending mode. Some so-called snubber cables (connected to the side walls of the wind-tunnel test section) are added to limit

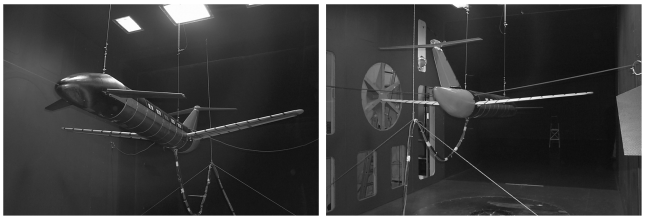

Fig. 18 X-DIA model equipped with VZLU canard with free–free suspension system.

maximum model excursion. A rear *Y* cable (see Fig. 18) is suspending the umbilical cable, which is connecting the model to the power supply, a control system computer, and a data acquisition system. Modal identification has been performed including this suspension system. Results are reported in Tables 2 and 3. The main difference between fuselage dynamic response on the component and the complete model is related to the fact that, in the free–free configuration, the complete model shows for the first vertical bending of fuselage a nodal point close to the foreplanes. This means that for that configurations, the advantages of AAMFP in damping fuselage bending are not so evident due to the loss of controllability of foreplane on the first bending fuselage mode. It is important to underline that this limit is mainly due to the presence of big masses represented by two electric motors and a belt-based driving system close to the attachment of foreplanes to the fuselage, and this limit is typical of the scale model and not of the full-scale aircraft. Otherwise, the wind-tunnel testing on the complete model could be useful to, test the capability of AAMFP concept in damping fuselage torsion. It is possible to see that in the case of VZLU foreplane two modes, No. 4 and No. 5, respectively, show a significant participation of fuselage torsion, as depicted in Fig. 20, whereas in the case of the DLR foreplane, only one main fuselage torsion mode is present in the frequency range 10–25 Hz (its shape is reported in Fig. 19). The main purpose of wind-tunnel testing on the complete model was the experimental verification of the capability of AAMFP control to increase damping on these three modes. During this test activity, accelerometers were used as well as rate gyros, which were added to identify rotational motion of the fuselage. In this case, excitation has been introduced on one side of the rear fuselage through a cable

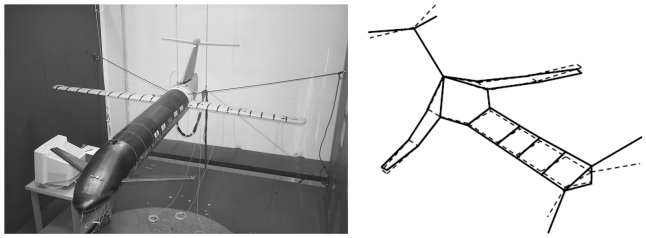

a) Modal testing setup **b) Mode shape no.6**

Fig. 19 Modal testing setup and mode shape no. 6 with DLR foreplane controlled during X-DIA complete model wind-tunnel testing.

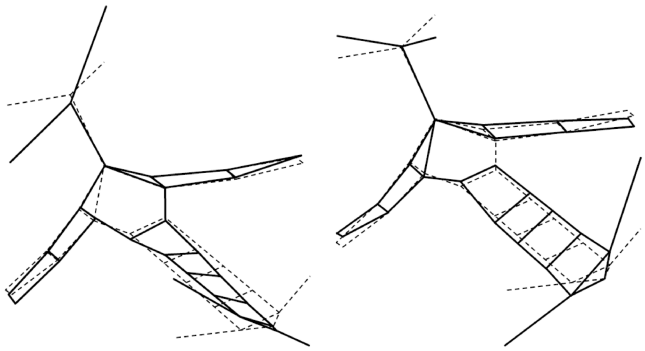

a) Mode shape no.4 **b) Mode shape no.5**

Fig. 20 Mode shapes nos. 4 and 5 damped by ILAF control during X-DIA complete model wind-tunnel testing.

connected to a long-stroke shaker, located outside the wind-tunnel test chamber. Even in this case, a stepped sine excitation, ranging from 10 to 25 Hz, has been applied. The control system adopted to move the foreplane surfaces is identical to one previously tested at VZLU. In this case, because in free–free configuration, fuselage torsion mode shows a frequency lower than in the case of front fuselage alone, the effectiveness of foreplane in increasing modal damping can be investigated. Similarly to what was reported for

Table 2 Airplane with VZLU canard installed

Mode no.	Frequency, Hz	Damping, %	Shape
1	7.25	0.81	First wing symm. bending
2	11.20	1.05	First wing symm. torsion
3	12.50	0.76	First wing antisymm. bending plus first fuselage torsion
4	16.12	1.70	First wing antisymm. torsion plus first fuselage torsion[a]
5	20.01	1.60	First wing antisymm. bending plus first fuselage torsion[b]
6	27.16	2.87	First fuselage bending plus tail plane
7	31.86	1.37	First wing antisymm. bending plus second fuselage torsion
8	34.03	2.16	First wing symm. bending plus first fuselage bending plus tail plane bending[c]

[a]Tailplane and wing in phase.
[b]Tailplane and wing counterphase.
[c]Fuselage and tail plane counterphase.

Table 3 Airplane with DLR canard installed

Mode no.	Frequency, Hz	Damping, %	Shape
1	7.02	1.06	First wing symm. bending
2	8.41	1.20	First wing antisymm. torsion
3	10.67	0.76	First wing symm. torsion
4	12.78	1.16	Rear fuselage bending plus tail plane
5	15.64	1.18	First wing symm. torsion plus first fuselage torsion
6	19.57	1.49	First wing antisymm. bending plus first fuselage torsion
7	22.62	0.50	First wing antisymm. bending plus fuselage torsion
8	27.43	2.44	First fuselage symm. bending plus tail plane bending[a]

[a]In phase.

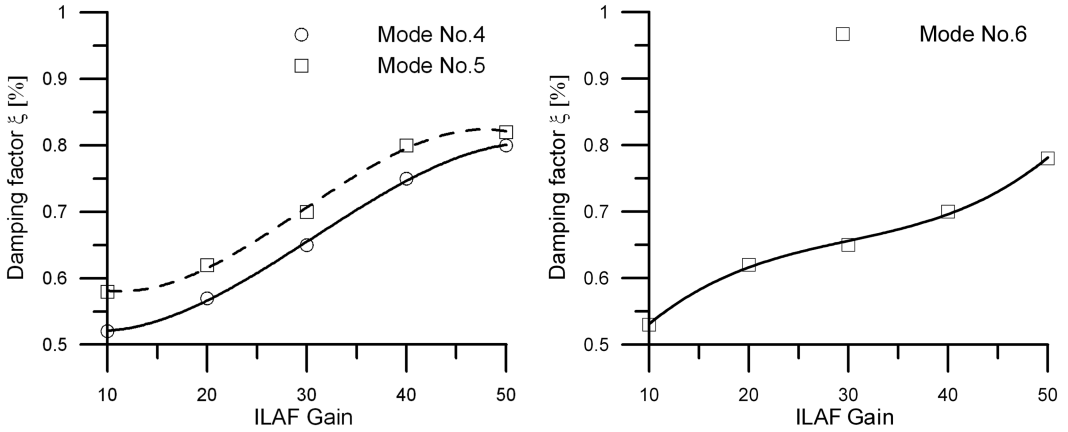

a) X-DIA complete model with VZLU fore planes **b) X-DIA complete model with DLR fore planes**

Fig. 21 Gain effectiveness measured during wind-tunnel test on complete X-DIA model.

component model testing, a gain effectiveness as a function of the antisymmetric control gain is shown in Fig. 21 for VZLU and DLR foreplanes, corresponding to a speed of 20 m/s. In fact, the first test campaign on the complete X-DIA model has been limited to this speed for sake of safety. Looking at these results, it is possible to underline the following comments. In the diagrams reporting VZLU foreplane results, the efficiency of AAMFP concept is demonstrated for both modes nos. 4 and 5, which show participation of fuselage torsion. For a gain ranging from 10 to 50, ILAF control grants an extra damping from about 0.5 to 0.8% for modes nos. 4 and 5. When using DLR foreplane, instead, only mode no. 6 shows the participation of fuselage torsion, and so this is the only one damped by asymmetric ILAF control. Indeed, for a gain ranging from 10 to 50, the obtained modal damping ranges from 0.5 to 0.7%, and so even in this case, it is possible to get to values similar to ones obtained for the VZLU foreplane. The AAMFP appears able to greatly improve damping of fuselage torsion, even in case of low speed. The differences on performances between these two type of foreplanes can be partly attributed to the lifting surface area and span (both lower for DLR).

VIII. Conclusions

The paper summarizes the activities related to aeroelastic active control performed in the framework of the 3AS European project aiming at investigating the capability of the active all-movable foreplane concept, coupled to an ILAF control scheme, to improve fuselage damping. For this purpose, both numerical and experimental activities have been carried out. In particular, an aeroelastic demonstrator, that is, a wind-tunnel aeroelastic model one-tenth geometrically and dynamically scaled with respect to a 100-seat reference liner showing a three-surface configuration, has been designed and manufactured. Two wind-tunnel test campaigns have been completed since now, one on front fuselage equipped with two kinds of foreplanes, and the second one on complete wind-tunnel model. It has been demonstrated that ILAF control worked very well symmetrically and antisymmetrically, showing remarkable reductions in fuselage bending and torsion for the sting-supported component model. In this configuration, the control system was able to introduce additional damping up to a value that reduced the foreplane tip accelerations by 50%. Both foreplane types showed similar results; slight differences were found only in control gains, but this fact is directly connected to the different sweep angles and planforms. During the tests on the complete airplane model, the control system still performed very satisfactorily: looking at the results obtained with VZLU foreplanes installed, it appears that not only can a specific torsion mode be damped by the installed system (control system and foreplane), but it is also able to spread its beneficial effect to at least two other modes with large participation of fuselage torsion. Peaks at approximately 16, 20, and 22 Hz are drastically improved, obtained simply by augmenting control system gain (i.e., tuning ILAF aggressiveness). The DLR foreplane configuration showed similar results. It is quite evident that the normal mode characteristics are largely modified by different local structural mass and by different global mass location (due to negative sweep angle). The highest damping is provided by the DLR foreplane at approximately 22 Hz. The effectiveness of the AAMFP concept analyzed in the 3AS project has been proven both by numerical and experimental results. Future research and development will continue on the X-DIA airplane configuration to investigate the interaction of an active all-movable foreplane and an active camber wing with regard to gust alleviation as well as aircraft flight mechanics.

Acknowledgments

The numerical and experimental activities related to the AAMFP concept applied to the X-DIA model were funded by the European Union under the Fifth Research Framework through the Active Aeroelastic Aircraft Structures project number GRD-1-2001-40122. The authors would like to thank Paolo Mantegazza and Giampiero Bindolino for their generous advice and Guiseppe Quaranta for his support in state-space aeroelastic modeling.

References

[1] Wykes, J., and Kordes, E., "Analytical Design and Flight Tests of a Modal Suppression System on the XB-70 Airplane: Part 1-Design Analysis, Part 2-Flight Tests," *AGARD Conference Proceedings, Aeroelastic Effects From a Flight Mechanics Standpoint , No. 46*, AGARD Paper 23, 1970.

[2] Lock, W., Kordes, E., McKay, J., and Wykes, J., "Flight Investigation of a Structural Mode Control System for XB-70 Aircraft," NASA TN D-7420, 1973.

[3] Dempster, J., and Roger, K., "Evaluation of B-52 Structural Response to Random Turbulence with Stability Augmentation Systems," *Journal of Aircraft*, Vol. 4, No. 6, 1967, pp. 507–515.

[4] Wykes, J. H., Kelpl, M. J., and Brosnan, M. J., "Flight test and Analyses of the B-1 Structural Mode Control System at Supersonic Flight Conditions," NASA CR 170405, 1983.

[5] Perry, B., and Cole, S. R., "Summary of an Active Flexible Wing Program," *Journal of Aircraft*, Vol. 32, No. 1, 1995, pp. 10–15; also AIAA Paper 92-2080, April 1992.

[6] Woods-Vedler, J. A., Pototzky, A., and Hoadley, S., "Rolling Maneuver Load Alleviation Using Active Control," *Journal of Aircraft*, Vol. 32, No. 1, 1995, pp. 68–76.

[7] Pendleton, E., Bessette, D., Field, P., Miller, G., and Griffin, K., "Active Aeroelastic Wing Flight Research Program: Technical Program and Model Analytical Development," *Journal of Aircraft*, Vol. 37, No. 4, 2000, pp. 554–561.

[8] Schweiger, H., and Suleman, A., "The European Research Project Active Aeroelastic Aircraft Structures," *Proceedings of the IFASD International Forum on Aeroelasticity*, CEAS/AIAA, Amsterdam, The Netherlands, 2003, pp. 1–10.

[9] Bindolino, G., Lanz, M., and Ricci, S., "X-DIA Program: Current Research Status," *Atti del XIII Congresso Nazionale*, Associazione Italiana di Aeronautica e Astronautica, Rome, 1995, pp. 1–12.

[10] Ricci, S., Scotti, A., and Zanotti, D., "Control of an All-Movable Foreplane for a Three Surfaces Aircraft Wind Tunnel Model Using Matlab/Simulink and RTAI Linux," *Mechanical Systems and Signal Processing*, Vol. 20, No. 5, July 2006, pp. 1044–1066. doi:10.1016/j.ymssp.2005.08.020

[11] Kendall, E. R., "The Minimum Induced Drag, Longitudinal Trim and Static Longitudinal Stability of Two Surface and Three Surface Airplanes," *Proceedings of the 2nd Applied Aerodynamics Conference*, AIAA, New York, 1984, pp. 1–11; also AIAA Paper 84-2164.

[12] Butler, G., "An Analytical Study of the Induced Drag of Canard Wing Tail Aircraft Configurations with Various Levels of Static Stability," *The Aeronautical Journal*, Vol. 87, No. 868, Oct. 1983, pp. 293–300.

[13] Selberg, B. P., and Kamran, R., "Aerodynamic Tradeoff Study of Conventional, Canard, and Tri-Surface Aircraft Systems," *Proceedings of the 3rd Applied Aerodynamics Conference*, AIAA, New York, 1985, pp. 1–20; also AIAA Paper 85-4071.

[14] Naik, D., and Ostowari, C., "Experimental Study of a Three Lifting Surface Configuration," *Journal of Aircraft*, Vol. 25, No. 2, Feb. 1988, pp. 106–112.

[15] Rae, W. H., and Pope, A., *Low Speed Wind Tunnel Testing*, Wiley, New York, 1984.

[16] Saltzman, E., and Hicks, J., "In-Flight Lift-Drag Characteristics for a Forward-Swept Wing Aircraft," NASA TP 3414, 1994.

[17] Scotti, A., Ricci, S., and Quaranta, G., "Active Control of a Three Surface Wind Tunnel Aeroelastic Demonstrator: Modelling and Correlations," *Proceedings of the IFASD International Forum on Aeroelasticity*, CEAS/AIAA, Paper IF-029, 2005, pp. 1–14.

[18] Vepa, R., "On the Use of Pade Approximants to Represent Unsteady Aerodynamic Loads for Arbitrarily Small Motions of Wings," AIAA, TR 76-17, 1976.

[19] Roger, K., "Airplane Math Modeling Methods for Active Control design," AGARD TR CP 228, 1977.

[20] Karpel, M., "Design for Active Flutter Suppression and Gust Alleviation Using State-Space Aeroelastic Modeling," *Journal of Aircraft*, Vol. 19, No. 3, 1982, pp. 221–227.

[21] Karpel, M., "Reduced Order Aeroelastic Models via Dynamic Residualization," *Journal of Aircraft*, Vol. 27, No. 5, 1990, pp. 449–455.

[22] Karpel, M., "Physically Weighted Approximation of Unsteady Aerodynamic Forces Using the Minimum-State Method," NASA TP 3025, 1991.

[23] Morino, L., Mastroddi, F., De Troia, F., Ghiringhelli, G. L., and Mantegazza, P., "Matrix Fraction Approach for Finite-State Aerodynamic Modeling," *AIAA Journal*, Vol. 33, No. 4, April 1995, pp. 703–711.

[24] Antoulas, A., and Sorensen, D., "Approximation of Large-Scale Dynamical Systems: An Overview," *International Journal of Applied Mathematics and Computer Science*, Vol. 11, No. 5, 2001, pp. 1093–1121.

[25] Moore, B. C., "Principal Component Analysis in Linear System: Controllability, Observability and Model Reduction," *IEEE Transactions on Automatic Control*, Vol. 26, No. 1, Feb. 1981, pp. 17–32. doi:10.1109/TAC.1981.1102568

[26] Pasinetti, G., and Mantegazza, P., "Single Finite States Modeling of Aerodynamic Forces Related to Structural Motions and Gusts," *AIAA Journal*, Vol. 37, No. 5, May 1999, pp. 604–612.

[27] Mantegazza, P., and Quaranta, G., "A Robust Technique to Create Reduced Order Models for Aircraft Aerodynamic Unsteady Loads," *Journal of Aircraft* (to be published).

[28] Malecek, J., Cecrdle, J., Scotti, A., Ricci, S., Kiessling, F., and Klimmek, T., "Dynamic Response Analysis and Experimental Validation of the X-DIA Demonstrator Component Model," *Proceedings of the IFASD International Forum on Aeroelasticity*, DGLR/CEAS/AIAA Paper IF-057, DGLR–Bericht, 2005, pp. 1–12, ISBN 3-932182-43-X.

[29] Malecek, J., "X-DIA Demonstrator Aeroelastic Test," *Proceedings of Engineering Mechanics*, Institute of Thermomechanics, Department of Sciences of Czech Republic, Svratka, Czech Republic, 2005, pp. 1–9, ISBN 80-85918-93-5.

[30] Cecrdle, J., "X-DIA Demonstrator Aeroelastic Test-Design, Analysis and Model Wind Tunnel Support Tuning," *Proceedings of the 45th AIAA/ASME/ASCE/AHS/ASC Structures, Structural Dynamics and Materials*, Institute of Thermomechanics, Department of Sciences of Czech Republic, Svratka, Czech Republic, 2005, pp. 1–9, ISBN 80-85918-93-5.

[31] Ricci, S., Scotti, A., and Malecek, J., Cecrdle, J., "Experimental Investigations of a Vibration Suppression System for a Three Surface Aeroelastic Model," *Proceedings of the 46th AIAA/ASME/ASCE/AHS/ASC SDM Conference*, AIAA, Reston, VA, 2005, pp. 1–17; also AIAA Paper 2005-2232

[32] Ricci, S., and Scotti, A., "Aeroelastic Testing of a Three Surface Aircraft," *Proceedings of the 47th AIAA/ASME/ASCE/AHS/ASC SDM Conference*, AIAA, Reston, VA, 2005, pp. 1–17; also AIAA Paper 2006-2189.